Nondipolar Asymmetries of Photoelectron Angular Distributions

B. Krässig, M. Jung, D. S. Gemmell, E. P. Kanter, T. LeBrun, S. H. Southworth, and L. Young
Physics Division, Argonne National Laboratory, Argonne, Illinois 60439
(Received 26 July 1995)

We have measured the nondipolar contribution to the Ar 1*s* photoelectron angular distribution over the 30–2000 eV electron-energy range. The nondipolar interaction results in a forward or backward asymmetry with respect to the photon beam. The asymmetry is directed backward near threshold, is symmetric near 230 eV, and becomes increasingly forward directed at higher energies. The measured asymmetries are in excellent agreement with theoretical calculations, which include interference between the electric-dipole and electric-quadrupole photoionization amplitudes.

PACS numbers: 32.80.Fb

Current understanding of atomic photoionization phenomena is largely based on the dipole approximation [1–4]. Within this approximation, the standard transition matrix element used to describe photoionization between initial and final states, $M_{if} = \langle f | \exp(i\mathbf{k} \cdot \mathbf{r})\boldsymbol{\varepsilon} \cdot \mathbf{p} | i \rangle$, is simplified. In this expression, $\exp(i\mathbf{k} \cdot \mathbf{r})\boldsymbol{\varepsilon}$ describes the photon field ($\mathbf{k}$ is the photon propagation vector, $\mathbf{r}$ is the electron position vector, and $\boldsymbol{\varepsilon}$ the photon polarization vector), and $\mathbf{p}$ is the electron momentum operator. In the dipole approximation, only the first term of the expansion $\exp(i\mathbf{k} \cdot \mathbf{r}) \approx 1 + i\mathbf{k} \cdot \mathbf{r} - \frac{1}{2}(\mathbf{k} \cdot \mathbf{r})^2 + \cdots$ is retained; thus $\exp(i\mathbf{k} \cdot \mathbf{r})$ is replaced by unity. At low photon energies, ≤ 1 keV, the approximation is well justified since $\mathbf{k} \cdot \mathbf{r} \ll 1$. At higher photon energies the dipole approximation becomes less accurate, although it remains widely used, e.g., in extended x-ray absorption fine structure (EXAFS) studies of solid-state materials [5]. Photoelectron angular distributions, in contrast to angle-integrated cross sections, are much more sensitive to nondipolar interactions due to the contributions of terms involving interference with the dominant electric-dipole amplitude. In this paper, we report measurements showing the breakdown of the dipole approximation in photoionization as evidenced by considerable modification of photoelectron angular distributions obtained using linearly polarized x-ray beams with energies in the approximate range of 3–5 keV.

In the dipole approximation, the differential cross section for photoionization of randomly oriented target atoms by a linearly polarized photon beam has the form

$$d\sigma/d\Omega = (\sigma/4\pi)[1 + \beta P_2(\cos\theta)], \qquad (1)$$

where σ is the angle-integrated cross section, θ is the angle between the photon polarization and photoelectron momentum vectors, $P_2(\cos\theta) = \frac{1}{2}(3\cos^2\theta - 1)$, and β is the "photoelectron asymmetry parameter." The dependence of σ and β on photon energy has motivated a large body of experimental and theoretical work [2–4,6]. Within this approximation, the photoelectron angular distribution has a simple form, depending only on the emission angle with respect to the polarization vector, and thus has reflection symmetry about the plane perpendicular to the photon propagation vector.

Additional multipoles of the photon-atom interaction will increasingly contribute as the photon energy increases [2,7]. The first-order correction to the dipole approximation is obtained by retaining the second term in the expansion $[\exp(i\mathbf{k} \cdot \mathbf{r}) = 1 + i\mathbf{k} \cdot \mathbf{r}]$ [2,8]. The $i\mathbf{k} \cdot \mathbf{r}$ term gives rise to magnetic dipole and electric-quadrupole transition amplitudes. These interfere with the dominant electric-dipole amplitude in expressions for the differential cross section [8–12]. Consequently, the photoelectron angular distribution has a more complicated form, depending not only on the angle of emission relative to the polarization vector but also on the angle relative to the photon propagation vector. Further insight into the angular symmetry properties of photoelectron angular distributions is obtained by considerations of angular momentum and parity, as in Peshkin's formulation for arbitrary multipolarity and polarization [9].

Breakdown of the dipole approximation was considered in very early experimental and theoretical work in which the emphasis was on high-energy x-ray excitation [1,13]. However, the only measurements of nondipolar photoelectron asymmetries using soft x rays have been the experiments of Krause and Wuilleumier obtained using unpolarized x-ray lines below 2000 eV [14]. Those early measurements showed small, but distinct, enhancements of photoelectron intensity in the forward direction with respect to the x-ray beam. At that time, calculation and measurement of the β parameter was of primary interest, and the nondipolar asymmetry was accounted for qualitatively by "correction factors for retardation" [14,15]. However, the measurements of Krause and Wuilleumier motivated the application of more exact theoretical models to nondipolar effects in photoionization [7]. More recently, several theoretical studies have been reported that derive the form of the differential cross section when nondipolar interactions are included and predict values of nondipolar asymmetry parameters for selected atomic subshells as functions of photon energy [8,11,12].

Here we report measurements of the nondipolar asymmetries of Ar 1*s* photoelectrons over the electron-energy

 0031-9007/95/75(26)/4736(4)$06.00

range 30–2000 eV (3236–5205 eV x-ray energy) obtained at beam line X-24A of the National Synchrotron Light Source. Our measured asymmetries are compared with the calculations of Cooper [8], who has included interference between the electric-dipole ($E1$) and electric-quadrupole ($E2$) photoionization amplitudes within a nonrelativistic central-potential model. The effects due to the magnetic dipole term are expected to be much smaller in this energy range and are neglected [8].

Using Cooper's notation, the differential cross section for photoionization (including interference between $E1$ and $E2$ terms) with a linearly polarized photon beam is

$$d\sigma/d\Omega = (\sigma/4\pi)[1 + \beta P_2(\cos\theta) + (\delta + \gamma\cos^2\theta)\sin\theta\cos\varphi], \quad (2)$$

where the nondipolar effects are characterized by two new asymmetry parameters, δ and γ. As shown in Fig. 1, θ is the polar angle of the photoelectron momentum vector $\mathbf{p}$ with respect to the photon polarization vector $\boldsymbol{\varepsilon}$, and φ is the azimuthal angle between the photon propagation vector $\mathbf{k}$ and the projection of $\mathbf{p}$ in the plane perpendicular to $\boldsymbol{\varepsilon}$. According to Eq. (2), the magnitude of the nondipolar terms is maximal in the forward ($\varphi = 0°$) and backward ($\varphi = 180°$) directions with respect to $\mathbf{k}$ and vanishes in the plane perpendicular to $\mathbf{k}$.

Our experimental strategy focused on measurement of nondipolar (forward and backward) asymmetries in photoelectron angular distributions and the elimination of dipole anisotropies. To eliminate the β dependence of the observed angular asymmetries, a rotatable 45° parallel-plate electron analyzer (PPA) was mounted at a fixed polar angle of $\theta = 54.7°$, where $P_2(\cos\theta) = 0$. The forward or backward asymmetry was then obtained by rotating the PPA 360° in φ, i.e., about the axis containing the photon polarization vector $\boldsymbol{\varepsilon}$. With this measurement geometry, the term in Eq. (2) dependent on the β parameter is set to zero, and rotation of the PPA in φ isolates the nondipolar parameters δ and γ,

$$I(\varphi) = 1 + (2/3)^{1/2}(\delta + \gamma/3)\cos\varphi . \quad (3)$$

A further simplification occurs for Ar $1s$ photoelectrons, where selection rules in the nonrelativistic central-potential model allow only $s \rightarrow p$ waves in the dipole matrix elements and $s \rightarrow d$ waves in the quadrupole matrix elements [8]. Consequently, $\beta = 2$ and $\delta = 0$, simplifying Eq. (3) to

$$I(\varphi) = 1 + (2/27)^{1/2}\gamma\cos\varphi . \quad (4)$$

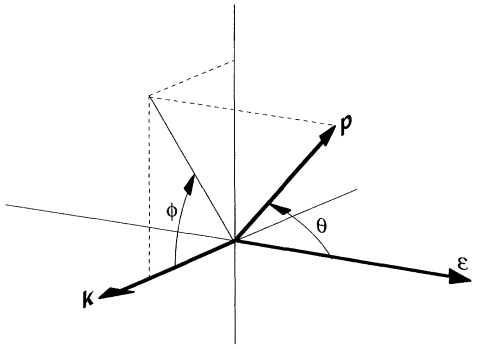

FIG. 1. Coordinates used for the description of photoelectron angular distributions: θ is the polar angle of the photoelectron momentum vector $\mathbf{p}$ with respect to the photon polarization vector ε, and ϕ is the azimuthal angle defined by the projection of $\mathbf{p}$ in the plane perpendicular to ε and containing the photon propagation vector $\mathbf{k}$.

The Ar gas target was produced by effusive flow from a 0.7 mm capillary tube positioned ≈1 mm below the intersection of the x-ray beam and rotation axis. Optical survey instruments were used to position the source of the PPA precisely on the rotation axis, (i.e., along the polarization vector $\boldsymbol{\varepsilon}$), and to define the propagation axis of the x-ray beam to be perpendicular to the rotation axis using two fixed apertures. A stationary cylindrical-mirror electron analyzer (CMA) was positioned opposite the rotatable PPA to provide a normalization signal for PPA data recorded at different angles. This normalization primarily accounted for variations in the x-ray beam intensity during data collection. For this purpose, the CMA monitored the relative intensity of Ar LMM Auger electrons. The CMA was also used to record excitation spectra with which to locate the Ar K edge [16] and calibrate the x-ray energy scale.

Measurements were made at photon energies from 30 to 2000 eV above the Ar $1s$ ionization energy at 3206.3 ± 0.3 eV [16]. Ge(111) crystals were used in the beam line's double-crystal monochromator, giving a bandwidth ≈2 eV in this energy range and a photon flux of $\approx 1 \times 10^{11}\text{s}^{-1}$ [17]. An aperture between the synchrotron radiation source and the beam line optics limited the vertical acceptance angle to 160 μrad and defined the polarization of the incident radiation. Theoretical expressions for the polarization properties of the synchrotron radiation source [18] were used to calculate that the radiation entering the beam line was ≈95% linearly polarized. The calculation ignored effects due to finite source size and assumed perfect alignment of the aperture and source point. The measured photoelectron angular distributions were consistent with a high degree (≈97%) of linear polarization.

There was an instrumental asymmetry due to the geometry of the interaction region. The ≈1 mm diameter x-ray beam passing through the effusive gas target produced an extended source that was not symmetric with respect to the PPA rotation axis. In addition, the PPA had finite angular acceptances of $\Delta\theta \approx 0.3°$ and $\Delta\varphi \approx 4.5°$. Therefore, the observed interaction volume varied as a function of the PPA angle, resulting in an instrumental anisotropy of ≈ ±10%. This instrumental asymmetry was determined by measuring the angular distributions of atomic and molecular Auger electrons that we assume to be emitted isotropically: Ne KLL, Ar KLL and LMM,

Kr *LMM*, Xe *MNN*, O *KVV* from CO_2, and N *KVV* from N_2. In the "two-step" model, Auger-electron angular distributions depend on the angular symmetry properties of the ensemble of vacancy-state magnetic sublevels produced in the photoionization step [6,19]. We expect the forward and backward asymmetries of the vacancy state distributions resulting from nondipolar interactions to be negligibly small in all cases. In addition, alignment due to dipolar photoionization is not possible for Ar 1*s* and Ne 1*s* vacancies, resulting in $\beta = 0$ for Ar *KLL* and Ne *KLL* Auger electrons. Nonzero β's are expected to be small in our low-resolution measurements, which average over several transitions, excited far above their respective thresholds. With the expectation that the Auger electrons are emitted isotropically, PPA angular scans were used to determine the instrumental asymmetry over a wide range of electron energies (≈200–2660 eV). These data were fitted and the resulting curves used to normalize PPA angular scans of Ar 1*s* photoelectrons.

A PPA angular scan consisted of 26 points taken over two complete revolutions in φ. The first (second) revolution sampled angles $0°, 30°, 60°, \ldots$ $(15°, 45°, 75°, \ldots)$. Typically, the dwell time per angle was 60 s. The PPA energy resolution was $\Delta E/E = 2\%$. For the Ar 1*s* photopeak, the count rate in the PPA was ≈20–50 Hz, whereas for the Auger electrons the count rates were considerably lower. In general, the angular scans of the Ar 1*s* photoelectrons were repeated ≈3 times and those of the Auger electrons repeated until ≈2% statistical accuracy was achieved.

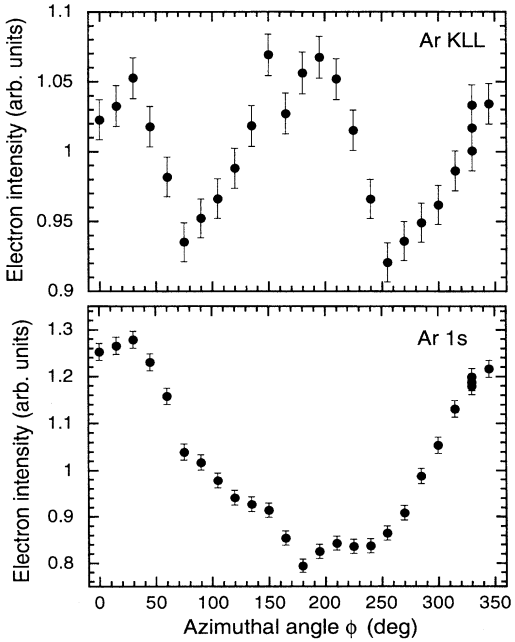

FIG. 2. Dependence on azimuthal angle ϕ of the intensities of 2660 eV Ar *KLL* Auger electron (top) and of 2000 eV Ar 1*s* photoelectrons (bottom) at fixed polar angle $\theta = 54.7°$ (the dipolar "magic angle").

Examples of PPA angular scans of Ar *KLL* Auger electrons at 2660 eV and Ar 1*s* photoelectrons at 2000 eV, normalized with respect to the CMA signal, are shown in Fig. 2. The Ar *KLL* data show an instrumental asymmetry of ≈ ±10%, with higher signal in the forward (0°) and backward (180°) directions than the up (90°) and down (270°) directions, as expected from the asymmetric source distribution. The Ar 1*s* data show a quite different angular dependence, with a strong (≈50%) enhancement in the forward direction compared to the backward. A smooth curve was fitted to the Ar *KLL* data and used to correct the Ar 1*s* data for the instrumental asymmetry.

The Ar 1*s* angular scan, corrected for instrumental asymmetry, is plotted in Fig. 3 along with a fitted curve. Here we note that Eq. (2) is correct only for complete polarization of the x-ray beam and for precise alignment of the rotation axis along the polarization vector. In analyzing the data, we accounted for the small deviations from these ideals by using a Stokes parameters approach [6,20] to describe the degree of polarization and the tilt angel between the rotation axis and the polarization ellipse. A detailed description of this work, the data analysis procedures, and results of measurements of nondipolar asymmetry parameters for Kr 2*s* and Kr 2*p* subshells is given in Ref. [21]. From the fit, a value for the nondipolar asymmetry parameter γ was determined. For each Ar 1*s* energy, a family of γ values was determined based upon the instrumental asymmetries derived from the various Auger-electron angular scans. The final γ values reported here are averages weighted by goodness of fit. The error bars reflect the spread in values given by the different instrumental corrections; statistical errors were small in comparison [21].

The measured γ values for Ar 1*s* are plotted in Fig. 4 along with Cooper's calculated results [8], and the agreement is excellent. The nondipolar asymmetry shows an interesting variation with energy; the asymmetry gives more intensity in the backward direction near threshold, vanishes near 230 eV, and becomes increasingly forward

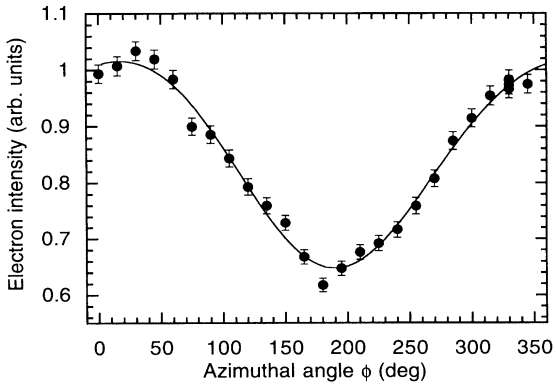

FIG. 3. Dependence on azimuthal angle ϕ of 2000 eV Ar 1*s* photoelectrons at fixed polar angle $\theta = 54.7°$ after correction for the instrumental asymmetry. The solid line is a fitted curve used to determine the nondipolar asymmetry parameter γ.

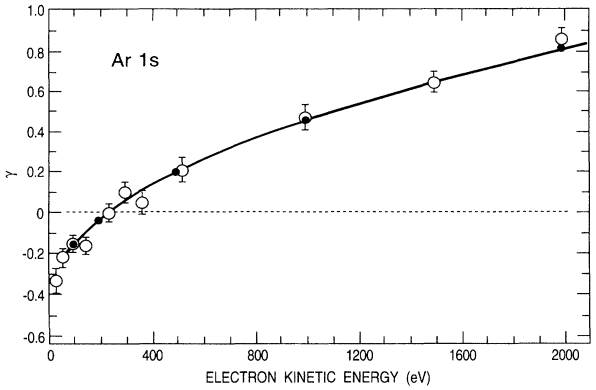

FIG. 4. Dependence on electron kinetic energy of measured values of the Ar 1s nondipolar asymmetry parameter γ (open circles) compared with Cooper's calculated values (solid circles with spline-fit line) [8].

directed at high energies. We note that the measurements (here and in Ref. [21]) confirm theoretical predictions [8,11,12] that different atomic subshells display different energy-dependent nondipolar asymmetries. The dependence of nondipolar asymmetries on energy and atomic subshell follows the theoretical formulation, which shows they are determined by the dipole and quadrupole radial matrix elements and continuum phase shifts [8].

In analogy to studies of the β parameter at lower energies [2–4,6], measurements of nondipolar asymmetries provide experimental tests of atomic photoionization theory at x-ray energies. With the advent of high-brilliance x-ray sources, we expect to explore theoretical predictions for higher-order multipole and relativistic effects as well as photon-photoelectron polarization correlations [22].

We thank C. Kurtz and B. Zabransky for excellent technical support and Dr. J. W. Cooper and Dr. M. Peshkin for discussions of the theoretical issues. We also thank Dr. P. M. Dehmer, Dr. J. L. Dehmer, and Dr. R. D. Deslattes for the loan of equipment. Measurements were made at the National Synchrotron Light Source, Brookhaven National Laboratory, which is supported by the U.S. Department of Energy, Division of Materials Sciences and Division of Chemical Sciences. This work was supported by the U.S. Department of Energy Office of Basic Sciences under Contract No. W-31-109-Eng-38.

[1] H. A. Bethe and E. E. Salpeter, *Quantum Mechanics of One- and Two-Electron Atoms* (Springer-Verlag, Berlin, 1957).
[2] S. T. Manson and D. Dill, in *Electron Spectroscopy: Theory, Techniques, and Applications,* edited by C. R. Brundle and A. D. Baker (Academic, New York, 1978), Vol. 2, pp. 157–195.
[3] A. F. Starace, in *Handbuch der Physik,* edited by W. Mehlhorn (Springer-Verlag, Berlin, 1982), Vol. XXXI, pp. 1–121.
[4] M. Ya. Amusia, *Atomic Photoeffect* (Plenum, New York, 1990).
[5] See, for example, T. M. Hayes and J. B. Boyce, Solid State Phys. **37**, 173 (1982).
[6] V. Schmidt, Rep. Prog. Phys. **55**, 1483 (1992).
[7] A. Ron, R. H. Pratt, and H. K. Tseng, Chem. Phys. Lett. **47**, 377 (1977); H. K. Tseng, R. H. Pratt, S. Yu, and A. Ron, Phys. Rev. A **17**, 1061 (1978).
[8] J. W. Cooper, Phys. Rev. A **47**, 1841 (1993).
[9] M. Peshkin, Adv. Chem. Phys. **18**, 1 (1970).
[10] M. Ya. Amusia and N. A. Cherepkov, *Case Studies in Atomic Physics* (North-Holland, Amsterdam, 1975), Vol. 5, pp. 47–179.
[11] A. Bechler and R. H. Pratt, Phys. Rev. A **39**, 1774 (1989); **42**, 6400 (1990).
[12] J. H. Scofield, Phys. Rev. A **40**, 3054 (1989); Phys. Scr. **41**, 59 (1990).
[13] H. Hall, Rev. Mod. Phys. **8**, 358 (1936).
[14] M. O. Krause, Phys. Rev. **177**, 151 (1969); F. Wuilleumier and M. O. Krause, Phys. Rev. A **10**, 242 (1974).
[15] J. W. Cooper and S. T. Manson, Phys. Rev. **177**, 157 (1969).
[16] M. Breinig, M. H. Chen, G. E. Ice, F. Parente, B. Crasemann, and G. S. Brown, Phys. Rev. A **22**, 520 (1980).
[17] P. L. Cowan, S. Brennan, R. D. Deslattes, A. Henins, T. Jach, and E. G. Kessler, Nucl. Instrum. Methods Phys. Res., Sect. A **246**, 154 (1986); P. L. Cowan, S. Brennan, T. Jach, D. W. Lindle, and B. A. Karlin, Rev. Sci. Instrum. **60**, 1603 (1989).
[18] K. J. Kim, in *X-Ray Data Booklet,* edited by D. Vaughn (Lawrence Berkeley Laboratory, Berkeley, CA, 1986), pp. 1–4.
[19] S. Flügge, W. Mehlhorn, and V. Schmidt, Phys. Rev. Lett. **29**, 7 (1972).
[20] V. Schmidt, Phys. Lett. **45A**, 63 (1973).
[21] M. Jung, B. Krässig, D. S. Gemmell, E. P. Kanter, T. LeBrun, S. H. Southworth, and L. Young (to be published).
[22] Y. S. Kim, I. B. Goldberg, and R. H. Pratt, Phys. Rev. A **51**, 424 (1995); **45**, 4542 (1992).